Available online at www.sciencedirect.com
ScienceDirect
Journal of Sound and Vibration 319 (2009) 1200–1221
JOURNAL OF SOUND AND VIBRATION
www.elsevier.com/locate/jsvi

Analytic formulation and numerical implementation of an acoustic pressure gradient prediction

Seongkyu Lee[a,*], Kenneth S. Brentner[a], F. Farassat[b], Philip J. Morris[a]

[a]*Department of Aerospace Engineering, The Pennsylvania State University, University Park, PA 16802, USA*
[b]*NASA Langley Research Center, Hampton, VA 23681, USA*

Received 29 November 2007; received in revised form 16 June 2008; accepted 17 June 2008
Handling Editior: S. Bolton
Available online 31 July 2008

Abstract

Two new analytical formulations of the acoustic pressure gradient have been developed and implemented in the PSU-WOPWOP rotor noise prediction code. The pressure gradient can be used to solve the boundary condition for scattering problems and it is a key aspect to solve acoustic scattering problems. The first formulation is derived from the gradient of the Ffowcs Williams–Hawkings (FW–H) equation. This formulation has a form involving the observer time differentiation outside the integrals. In the second formulation, the time differentiation is taken inside the integrals analytically. This formulation avoids the numerical time differentiation with respect to the observer time, which is computationally more efficient. The acoustic pressure gradient predicted by these new formulations is validated through comparison with available exact solutions for a stationary and moving monopole sources. The agreement between the predictions and exact solutions is excellent. The formulations are applied to the rotor noise problems for two model rotors. A purely numerical approach is compared with the analytical formulations. The agreement between the analytical formulations and the numerical method is excellent for both stationary and moving observer cases.

1. Introduction

Acoustic scattering of the noise generated by rotating blades is an area of research that is not well developed. For example, a helicopter fuselage, a tiltrotor wing, or the duct surrounding a fan, each may substantially modify the acoustic signal that arrives at an arbitrary observer location. Such a modification would change both the magnitude and directivity of the acoustic signal from what would be observed for an isolated rotor. The effect of a fuselage on the noise field generated by a rotating point source was demonstrated by Atalla and Glegg [1,2] using a ray-acoustics approach. Laik and Morris [3] showed a direct simulation of acoustic scattering by two- and three-dimensional bodies using an extension of the impedance mismatch method.

*Corresponding author. Tel.: +1 814 865 1989; fax: +1 814 865 1991.
E-mail addresses: sxl348@psu.edu (S. Lee), ksbrentner@psu.edu (K.S. Brentner), feri.farassat@nasa.gov (F. Farassat), pjmaer@engr.psu.edu (P.J. Morris).

0022-460X/$ - see front matter © 2008 Elsevier Ltd. All rights reserved.
doi:10.1016/j.jsv.2008.06.028

Tools exist for predicting fan noise scattering in turbofan engines, but only limited work has been done on the acoustic scattering of rotor noise by short ducts (i.e., ducted tail rotors, ducted propellers for compound rotorcraft, ducted fans in UAVs, etc.) The various numerical approaches [4–6] to solve the acoustic scattering problem use the acoustic velocity on a scattering surface as a boundary condition. For example, a rigid surface requires either the satisfaction of the impenetrability condition on the surface or zero normal acoustic velocity relative to the scattering surface. Most conventional acoustic codes compute acoustic pressure at an observer, not the acoustic velocity, but the gradient of the acoustic pressure is related to the acoustic velocity through the linearized momentum equation. As result, the boundary condition for the stationary scattering surface can be written as $\nabla p'_s \cdot \mathbf{n} = -\nabla p'_i \cdot \mathbf{n}$, where p'_i is the incident acoustic pressure and p'_s is the scattered pressure. The calculation of the acoustic pressure gradient is, therefore, a key aspect in solving acoustic scattering problems. A numerical evaluation of the pressure gradient, which requires evaluation of the spatial derivative of acoustic pressure with respect to each direction, is the simplest way to calculate the pressure gradient on the surface. Nevertheless, it is computationally expensive. Therefore, it is not practical to calculate the pressure gradient numerically for a realistic helicopter configuration, where the scattering computation may require the acoustic pressure gradient at thousands or even tens of thousands of collocation points on the scattering surface. Furthermore, for the complicated source (rotating blades) and scattering surfaces (complete helicopter configuration), it is not easy to obtain the pressure gradient numerically. Therefore, it is important to develop an analytical formulation for the pressure gradient to enable routine acoustic scattering predictions.

2. Research objective

The Ffowcs Williams–Hawking (FW–H) equation [7] is a powerful tool to solve acoustic propagation from arbitrary moving sources such as rotating blades. In this paper, analytic formulations for the pressure gradient are derived starting with the FW–H equation for general moving sources and eventually applied to rotor noise.

The analytical formulations have several distinct advantages in terms of numerical computation. First, no additional input data are needed to predict the acoustic pressure gradient beyond what is already required to predict acoustic pressure (or at most, numerical differentiation of the input data). Second, the retarded time algorithms that will be used have been refined and thoroughly tested in various numerical implementations of formulation 1A, which is a retarded-time integral representation of the solution of the FW–H equation. Finally, by computing the acoustic pressure gradient analytically, rather than using a purely numerical approach, significant computation savings (in terms of computer run time and memory) and increased robustness are expected. Furthermore, the computation of the acoustic pressure from the isolated rotor can be computed concurrently with the acoustic pressure gradient.

The goals of this paper are as follows:

1. Develop a computationally efficient analytical formulation for the acoustic pressure gradient to provide accurate input data for the boundary condition for the scattering problems.
2. Validate the formulation by comparison with available exact solutions.
3. Apply the formulation to the rotor noise cases.

3. Acoustic pressure gradient formulations

The PSU-WOPWOP rotor noise prediction code [8–10] is used in this work to predict the rotor noise (acoustic pressure), as well as the gradient of the acoustic pressure on the scattering body. The PSU-WOPWOP code is based on Farassat's formulation 1A [11,12]. A brief review is given in the next section.

3.1. Formulation 1A

Farassat's formulation 1A [11,12] is an integral representation of the solution to the FW–H equation, without the quadrupole source term. It is a retarded-time formulation, which can be written as

$$p'(\mathbf{x},t) = p'_T(\mathbf{x},t) + p'_L(\mathbf{x},t), \tag{1}$$

where p', p'_T, and p'_L denote the acoustic pressure, the monopole source, and the dipole source. When the acoustic data surface coincides to the actual impenetrable surface, the last two terms become the thickness and loading components of the acoustic pressure, respectively. The monopole noise contribution p'_T can be written as

$$4\pi p'_T(\mathbf{x},t) = \int_{f=0} \left[\frac{\rho_0(\dot{U}_n + U_{\dot{n}})}{r(1-M_r)^2}\right]_{\text{ret}} \mathrm{d}S + \int_{f=0} \left[\frac{\rho_0 U_n(r\dot{M}_r + c(M_r - M^2))}{r^2(1-M_r)^3}\right]_{\text{ret}} \mathrm{d}S, \tag{2}$$

while the dipole noise contribution p'_L is written as

$$\begin{aligned} 4\pi p'_L(\mathbf{x},t) = {} & \frac{1}{c}\int_{f=0} \left[\frac{\dot{L}_r}{r(1-M_r)^2}\right]_{\text{ret}} \mathrm{d}S + \int_{f=0} \left[\frac{L_r - L_M}{r^2(1-M_r)^2}\right]_{\text{ret}} \mathrm{d}S \\ & + \frac{1}{c}\int_{f=0} \left[\frac{L_r(r\dot{M}_r + c(M_r - M^2))}{r^2(1-M_r)^3}\right]_{\text{ret}} \mathrm{d}S, \end{aligned} \tag{3}$$

where $(\mathbf{x},t)$ and $(\mathbf{y},\tau)$ are the observer and source space–time variables, respectively, $r = |\mathbf{x}-\mathbf{y}|$ and c is the speed of sound in the undisturbed medium. The data surface is described implicitly by the equation $f(\mathbf{y},\tau) = 0$, where $f(\mathbf{y},\tau)$ is defined in such a way that $\nabla f = \hat{\mathbf{n}}$, which is the unit outward normal to the data surface with components n_i. The density of the undisturbed medium is ρ_0. In Eqs. (2) and (3) the subscripts r, n and M imply the dot product of the vector with either the unit vector in the radiation direction $\hat{\mathbf{r}}$, outward normal vector $\hat{\mathbf{n}}$ to the surface $f = 0$, or the surface Mach number $\mathbf{M}$, respectively. The dot over a variable indicates source time differentiation. The variables U_i and L_i are defined by

$$U_i = [1 - (\rho/\rho_0)]v_i + (\rho u_i/\rho_0), \tag{4}$$

$$L_i = P_{ij}\hat{n}_j + \rho u_i(u_n - v_n), \tag{5}$$

where u_i are the components of the local flow velocity vector and v_i are the components of the local blade surface velocity vector and P_{ij} is the compressive stress tensor. Eqs. (4) and (5) are the form used for a permeable surface, which is useful if the flow field around the rotor blades becomes transonic—as is the case for high-speed-impulsive noise. Eqs. (1)–(3) omit the quadrupole term in the FW–H equation, so all significant nonlinear sources should be contained within a permeable surface. This enables the inclusion of the contribution of those sources without carrying out a volume integration. For an impermeable surface, such as the actual blade surface, $U_i = v_i$ and $L_i = P_{ij}\hat{n}_j$.

3.2. Formulation G1

Taking the gradient of Eqs. (2) and (3) directly involves complicated algebraic manipulations. It is easier to start with the partial differential equation form of the FW–H equation and then use the free-space Green's function to derive the new integral formulation. Details of this approach can be found in Ref. [13]. In this paper, the formulation is revisited with slightly different notation.

The acoustic pressure gradient can be found by taking the gradient of the FW–H monopole and dipole noise terms (neglecting the quadrupole source). The gradient of Eq. (1) is

$$\nabla p' = \nabla p'_T + \nabla p'_L. \tag{6}$$

The next step is to find the acoustic pressure gradient of the monopole and dipole noise sources. The governing equation for the monopole noise is

$$\Box^2 p'_T = \frac{\partial}{\partial t}[\rho_o U_n \delta(f)], \tag{7}$$

where $\delta(f)$ is the Dirac delta function with support on the data surface $f = 0$. Using the free-space Green's function $\delta(g)/4\pi r$, where $g = \tau - t + r/c$, the monopole component of pressure can be expressed as

$$4\pi p'_T(\mathbf{x}, t) = \frac{\partial}{\partial t}\int_{-\infty}^{t}\int_{-\infty}^{\infty}\frac{\rho_0 U_n}{r}\delta(f)\delta(g)\,\mathrm{d}\mathbf{y}\,\mathrm{d}\tau. \tag{8}$$

Taking the gradient of Eq. (8) yields

$$\begin{aligned} 4\pi\nabla p'_T(\mathbf{x}, t) &= \nabla\frac{\partial}{\partial t}\int_{-\infty}^{t}\int_{-\infty}^{\infty}\frac{\rho_0 U_n}{r}\delta(f)\delta(g)\,\mathrm{d}\mathbf{y}\,\mathrm{d}\tau \\ &= \frac{\partial}{\partial t}\int_{-\infty}^{t}\int_{-\infty}^{\infty}\rho_0 U_n\delta(f)\nabla_x\left(\frac{\delta(g)}{r}\right)\mathrm{d}\mathbf{y}\,\mathrm{d}\tau, \end{aligned} \tag{9}$$

where the symbol ∇_x stands for gradient operator with respect to the observer variable $\mathbf{x}$. The spatial gradient operator can replaced by a time derivative using the relation

$$\nabla_x\left(\frac{\delta(g)}{r}\right) = -\frac{1}{c}\frac{\partial}{\partial t}\left(\frac{\hat{\mathbf{r}}\delta(g)}{r}\right) - \frac{\hat{\mathbf{r}}\delta(g)}{r^2}. \tag{10}$$

Combining Eqs. (9) and (10) yields

$$4\pi\nabla p'_T(\mathbf{x}, t) = -\frac{\partial}{\partial t}\left(\frac{1}{c}\frac{\partial}{\partial t}\int_{-\infty}^{t}\int_{-\infty}^{\infty}\frac{\hat{\mathbf{r}}\rho_0 U_n}{r}\delta(f)\delta(g)\,\mathrm{d}\mathbf{y}\,\mathrm{d}\tau + \int_{-\infty}^{t}\int_{-\infty}^{\infty}\frac{\hat{\mathbf{r}}\rho_0 U_n}{r^2}\delta(f)\delta(g)\,\mathrm{d}\mathbf{y}\,\mathrm{d}\tau\right). \tag{11}$$

Using generalized function theory and geometry [14–16]—and following the same steps Farassat used in deriving formulation 1A—the gradient of the monopole component of the acoustic pressure is found to be

$$4\pi\nabla p'_T(\mathbf{x}, t) = -\frac{\partial}{\partial t}\left(\frac{1}{c}\frac{\partial}{\partial t}\int_{f=0}\left[\frac{\hat{\mathbf{r}}\rho_0 U_n}{r(1-M_r)}\right]_{\mathrm{ret}}\mathrm{d}S + \int_{f=0}\left[\frac{\hat{\mathbf{r}}\rho_0 U_n}{r^2(1-M_r)}\right]_{\mathrm{ret}}\mathrm{d}S\right) = -\frac{\partial E_1}{\partial t}. \tag{12}$$

By recalling that

$$\frac{\partial}{\partial t}[\ldots]\Big|_{\mathbf{x}} = \left[\frac{1}{1-M_r}\frac{\partial}{\partial\tau}[\ldots]\Big|_{\mathbf{x}}\right]_{\mathrm{ret}} \tag{13}$$

and

$$\frac{\partial\hat{\mathbf{r}}}{\partial\tau} = \frac{c}{r}(M_r\hat{\mathbf{r}} - \mathbf{M}), \tag{14}$$

it can be easily shown that

$$E_1 = \frac{1}{c}\int_{f=0}[\hat{\mathbf{r}}E_T]_{\mathrm{ret}}\,\mathrm{d}S + \int_{f=0}\left[\frac{(\hat{\mathbf{r}} - \mathbf{M})\rho_0 U_n}{r^2(1-M_r)^2}\right]_{\mathrm{ret}}\mathrm{d}S, \tag{15}$$

where

$$E_T = \left[\frac{\rho_0(\dot{U}_n + U_{\dot{n}})}{r(1-M_r)^2}\right]_{\mathrm{ret}} + \left[\frac{\rho_0 U_n(r\dot{M}_r + c(M_r - M^2)}{r^2(1-M_r)^3}\right]_{\mathrm{ret}} \tag{16}$$

is the combined monopole noise integrand in formulation 1A. Hence, it is already available in the noise prediction code. Finally, the monopole component of the acoustic pressure gradient can be written as

$$4\pi\nabla p'_T(\mathbf{x},t) = -\frac{\partial}{\partial t}\left\{\frac{1}{c}\int_{f=0}[\hat{\mathbf{r}}E_T]_{\text{ret}}\,\mathrm{d}S + \int_{f=0}\left[\frac{(\mathbf{r}-\mathbf{M})\rho_0 U_n}{r^2(1-M_r)^2}\right]_{\text{ret}}\mathrm{d}S\right\}. \tag{17}$$

The observer time derivative of the two integrals can be determined numerically.

The derivation of the gradient of the dipole noise component of the acoustic pressure follows the same procedure as used in the monopole noise component. The governing equation for the dipole noise is written as

$$\Box^2 p'_L = -\nabla\cdot[\mathbf{L}\delta(f)], \tag{18}$$

thus the dipole component of acoustic pressure is

$$4\pi p'_L(\mathbf{x},t) = -\nabla\cdot\int_{-\infty}^{t}\int_{-\infty}^{\infty}\frac{\mathbf{L}}{r}\delta(f)\delta(g)\,\mathrm{d}\mathbf{y}\,\mathrm{d}\tau = -\int_{-\infty}^{t}\int_{-\infty}^{\infty}\delta(f)\mathbf{L}\cdot\nabla_x\left(\frac{\delta(g)}{r}\,\mathrm{d}\mathbf{y}\,\mathrm{d}\tau\right). \tag{19}$$

Using Eq. (10) in the previous integral yields

$$4\pi p'_L(\mathbf{x},t) = \frac{1}{c}\frac{\partial}{\partial t}\int_{-\infty}^{t}\int_{-\infty}^{\infty}\frac{L_r}{r}\delta(f)\delta(g)\,\mathrm{d}\mathbf{y}\,\mathrm{d}\tau + \int_{-\infty}^{t}\int_{-\infty}^{\infty}\frac{L_r}{r^2}\delta(f)\delta(g)\,\mathrm{d}\mathbf{y}\,\mathrm{d}\tau. \tag{20}$$

Then if the gradient of the dipole component of acoustic pressure is taken, the result is

$$4\pi\nabla p'_L(\mathbf{x},t) = \frac{1}{c}\frac{\partial}{\partial t}\int_{-\infty}^{t}\int_{-\infty}^{\infty}\delta(f)\mathbf{L}\cdot\nabla_x\left(\frac{\hat{\mathbf{r}}\delta(g)}{r}\right)\mathrm{d}\mathbf{y}\,\mathrm{d}\tau + \int_{-\infty}^{t}\int_{-\infty}^{\infty}\delta(f)\mathbf{L}\cdot\nabla_x\left(\frac{\hat{\mathbf{r}}\delta(g)}{r^2}\right)\mathrm{d}\mathbf{y}\,\mathrm{d}\tau. \tag{21}$$

Note that the observer and the source space–time variables are independent because none of the Dirac delta functions have been used yet in the integration. This approach makes it easy to interpret the differential operators. Had the integrated results been used, heavy algebraic manipulations would be needed and the differential operators would require careful interpretation.

Using the following relations

$$\mathbf{L}\cdot\nabla_x\left(\frac{\hat{\mathbf{r}}\delta(g)}{r}\right) = \mathbf{L}\cdot\nabla_x\left(\frac{\hat{\mathbf{r}}}{r}\right)\delta(g) + \frac{L_r\hat{\mathbf{r}}}{cr}\delta'(g) = \frac{\mathbf{L}-2L_r\hat{\mathbf{r}}}{r^2}\delta(g) - \frac{L_r\hat{\mathbf{r}}}{cr}\frac{\partial}{\partial t}\delta(g), \tag{22}$$

$$\mathbf{L}\cdot\nabla_x\left(\frac{\hat{\mathbf{r}}\delta(g)}{r^2}\right) = \mathbf{L}\cdot\nabla_x\left(\frac{\hat{\mathbf{r}}}{r^2}\right)\delta(g) + \frac{L_r\hat{\mathbf{r}}}{cr^2}\delta'(g) = \frac{\mathbf{L}-3L_r\hat{\mathbf{r}}}{r^3}\delta(g) - \frac{L_r\hat{\mathbf{r}}}{cr^2}\frac{\partial}{\partial t}\delta(g), \tag{23}$$

leads to

$$\begin{aligned}4\pi\nabla p'_L(\mathbf{x},t) = \frac{1}{c}\frac{\partial}{\partial t}&\left\{-\frac{1}{c}\frac{\partial}{\partial t}\int_{-\infty}^{t}\int_{-\infty}^{\infty}\frac{L_r\hat{\mathbf{r}}}{r}\delta(f)\delta(g)\,\mathrm{d}\mathbf{y}\,\mathrm{d}\tau + \int_{-\infty}^{t}\int_{-\infty}^{\infty}\frac{(\mathbf{L}-3L_r\hat{\mathbf{r}})}{r^2}\delta(f)\delta(g)\,\mathrm{d}\mathbf{y}\,\mathrm{d}\tau\right\}\\ &+\int_{-\infty}^{t}\int_{-\infty}^{\infty}\frac{(\mathbf{L}-3L_r\hat{\mathbf{r}})}{r^3}\delta(f)\delta(g)\,\mathrm{d}\mathbf{y}\,\mathrm{d}\tau.\end{aligned} \tag{24}$$

Again following the procedure used for formulation 1A, Eq. (24) can be rewritten as

$$\begin{aligned}4\pi\nabla p'_L(\mathbf{x},t) = \frac{1}{c}\frac{\partial}{\partial t}&\left\{-\frac{1}{c}\int_{f=0}\left[\frac{1}{1-M_r}\frac{\partial}{\partial\tau}\left(\frac{L_r\hat{\mathbf{r}}}{r(1-M_r)}\right)\right]_{\text{ret}}\mathrm{d}S\right.\\ &\left.+\int_{f=0}\left[\frac{\mathbf{L}-3L_r\hat{\mathbf{r}}}{r^2(1-M_r)}\right]_{\text{ret}}\mathrm{d}S\right\}+\int_{f=0}\left[\frac{\mathbf{L}-3L_r\hat{\mathbf{r}}}{r^3(1-M_r)}\right]_{\text{ret}}\mathrm{d}S.\end{aligned} \tag{25}$$

Simplifying Eq. (25) gives the gradient of the dipole noise component of the acoustic pressure

$$4\pi\nabla p'_L(\mathbf{x},t)=\frac{1}{c}\frac{\partial}{\partial t}\left\{-\int_{f=0}[\hat{\mathbf{r}}E_L]_{\text{ret}}\,\mathrm{d}S+\int_{f=0}\left[\frac{\mathbf{L}-L_r\hat{\mathbf{r}}}{r^2(1-M_r)}\right]_{\text{ret}}\mathrm{d}S-\int_{f=0}\left[\frac{L_r\hat{\mathbf{r}}-L_r\mathbf{M}}{r^2(1-M_r)^2}\right]_{\text{ret}}\mathrm{d}S\right\}+\int_{f=0}\left[\frac{\mathbf{L}-3L_r\hat{\mathbf{r}}}{r^3(1-M_r)}\right]_{\text{ret}}\mathrm{d}S, \tag{26}$$

where E_L is the combined dipole noise integrand in formulation 1A

$$E_L=\frac{1}{c}\left[\frac{\dot{L}_r}{r(1-M_r)^2}\right]_{\text{ret}}+\left[\frac{L_r-L_M}{r^2(1-M_r)^2}\right]_{\text{ret}}+\frac{1}{c}\left[\frac{L_r(r\dot{M}_r+c(M_r-M^2))}{r^2(1-M_r)^3}\right]_{\text{ret}}. \tag{27}$$

Again, the observer time derivative in Eq. (26) needs to be taken numerically.

For convenience, Eqs. (17) and (26) are together referred to as formulation G1. This notation parallels that used by Farassat for the monopole and dipole formulation 1, which had a observer time derivative outside of the integrals. Evaluation of the pressure gradient can now be completed with substantially less computational effort than a direct numerical evaluation of the pressure gradient.

Eqs. (17) and (26) have been implemented in the PSU-WOPWOP noise prediction code to provide the acoustic pressure gradient at an arbitrary observer location. The main challenge of this implementation is the calculation of observer time derivative, $\partial/\partial t$, of the integrals. Care must be taken to ensure that the observer position $\mathbf{x}$ remains fixed during the calculation of these integrals. To simplify the algorithm description, the integrals which must be differentiated, surrounded by the braces in Eq. (26), are represented by Q. A second-order backward difference algorithm is used to compute the time derivative. The general algorithm for the numerical calculation of $\partial/\partial t$ is as follows:

A. Pick τ^n—n indicates time step and τ represents the emission or retarded time.
B. Compute $\mathbf{y}_i(\tau^n)$—each source point is moving, thus at time n, the position of the i-th source point is needed.
C. Save τ^n, $\mathbf{y}_i(\tau^n)$, velocity, acceleration, etc. for later use as the τ^{n-1} and τ^{n-2} values once n has been incremented.
D. Compute $\mathbf{x}(t^n)$ (based on $\mathbf{y}_i(\tau^n)$ and τ^n)—if $\mathbf{x}$ does not change (i.e., a stationary observer) , then the arrival time t is found explicitly by $t=\tau+r/c$; if the observer is moving, both the observer position and arrival (observer) time must be determined implicitly at the same time.
E. Calculate $Q(\mathbf{y}_i,\tau^n;\mathbf{x}(t^n),t^n_{x^n})\equiv Q^n_n$ using velocity, acceleration, etc. at τ^n.
F. Compute $t^{n-1}_{x^n}$ and $t^{n-2}_{x^n}$ using τ^{n-1} and τ^{n-2} as follows:
   (i) $t^{n-1}_{x^n}=\tau^{n-1}+|\mathbf{x}(t^n)-\mathbf{y}_i(\tau^{n-1})|/c$,
   (ii) $t^{n-2}_{x^n}=\tau^{n-2}+|\mathbf{x}(t^n)-\mathbf{y}_i(\tau^{n-2})|/c$.

   (If $\mathbf{x}$ is stationary, the calculation is simpler.)
G. Calculate $Q(\mathbf{y}^{n-1}_i,\tau^{n-1};\mathbf{x}(t^n),t^{n-1}_{x^n})\equiv Q^{n-1}_n$ and $Q(\mathbf{y}^{n-2}_i,\tau^{n-2};\mathbf{x}(t^n),t^{n-2}_{x^n})\equiv Q^{n-2}_n$.
H. Calculate

$$\frac{\partial Q}{\partial t}\cong\frac{Q^{n-2}_n-(1+\alpha)^2Q^{n-1}_n+\alpha(\alpha+2)Q^n_n}{\alpha(1+\alpha)(t^n_n-t^{n-1}_n)}\quad\text{where }\alpha=\frac{t^{n-1}_n-t^{n-2}_n}{t^n_n-t^{n-1}_n}$$

   for a non-uniform time step.
I. Interpolate $\partial Q/\partial t$ at t^*,

where τ denotes source time, t observer time, $\mathbf{y}_i$ source vector, $\mathbf{x}_i$ observer vector, c speed of sound, n time index and t^* is the specified observer time of interest. It is apparent that this procedure is significantly more complicated than computing the acoustic pressure. Nevertheless, the additional computational effort will be shown to be significantly less than a purely numerical differentiation of the acoustic pressure.

3.3. Formulation G1A

The primary drawback of formulation G1 is that numerical time differentiation of the integrals is required. If the observer is stationary, then this requirement is not a problem because the time history of the integrals can be easily differentiated numerically. If the observer is moving with respect to the fluid, as in the case of a wind-tunnel test, the situation becomes more complicated because the formulation requires the observer to be stationary during the evaluation of the integrals. Predictions with a moving observer are possible by adjusting the observer position at each time in the acoustic-pressure time history; however, three evaluation of the integrals are needed to perform a second-order difference approximation to the time derivatives at each observer time. These extra integral evaluations become unnecessary if the time derivatives are taken inside the integrals analytically.

Although the process of taking the observer time derivatives inside the integrals and converting them to source time derivatives is not difficult, it is quite tedious. The first step is to apply Eq. (13) and then evaluate the source time derivatives that results. Some of the key source time derivatives, which are the same as Farassat used in the derivation of formulation 1A, are expressed as follows:

$$\frac{\partial \hat{\mathbf{r}}}{\partial \tau} = \frac{c}{r}(M_r \hat{\mathbf{r}} - \mathbf{M}), \tag{28}$$

$$\frac{\partial r}{\partial \tau} = -cM_r, \tag{29}$$

$$\frac{\partial}{\partial \tau}\left(\frac{1}{r}\right) = -\frac{1}{r^2}\frac{\partial r}{\partial \tau} = \frac{cM_r}{r^2}, \tag{30}$$

$$\frac{\partial M_r}{\partial \tau} = \frac{c}{r}(-M^2 + M_r^2) + \dot{M}_r, \tag{31}$$

$$\frac{\partial L_r}{\partial \tau} = \dot{L}_r + \frac{c}{r}(M_r L_r - L_M). \tag{32}$$

Some new functions are introduced denoted by the following groups of variables:

$$W = r\dot{M}_r + c(M_r - M^2), \tag{33}$$

$$\dot{W} = \frac{r^2 \ddot{M}_r - 3cr\dot{\mathbf{M}} \cdot \mathbf{M} + c(r\dot{M}_r + c(M_r^2 - M^2))}{r}, \tag{34}$$

$$U(m,n) = \frac{1}{r^m (1 - M_r)^n}, \tag{35}$$

$$V(m,n) = \frac{\partial U(m,n)}{\partial \tau} = \frac{nr\dot{M}_r + (n-m)cM_r^2 + mcM_r - ncM^2}{r^{m+1}(1 - M_r)^{n+1}}, \tag{36}$$

or

$$V(m,n) = nWU(m+1, n+1) + c(m-n)M_r U(m+1, n). \tag{37}$$

These relations will be used in the process of taking the observer time derivatives inside the integrals in formulation G1.

Eqs. (17) and (26) are the starting point for the derivation of formulation G1A. Converting the observer time derivative to a source time derivative and using the new variables represented by Eqs. (34) and (35),

Eqs. (17) and (26) become

$$4\pi\nabla p'_T(\mathbf{x},t) = -\frac{1}{c}\int_{f=0}\left[\frac{1}{1-M_r}\frac{\partial}{\partial\tau}\{\hat{\mathbf{r}}(\dot{Q}U(1,2)+QWU(2,3))\}\right]_{\text{ret}}\mathrm{d}S - \int_{f=0}\left[\frac{1}{1-M_r}\frac{\partial}{\partial\tau}\{(\hat{\mathbf{r}}-\mathbf{M})QU(2,2)\}\right]_{\text{ret}}\mathrm{d}S, \tag{38}$$

$$\begin{aligned}4\pi\nabla p'_L(\mathbf{x},t) = &-\frac{1}{c}\int_{f=0}\left[\frac{1}{1-M_r}\frac{\partial}{\partial\tau}\left\{\hat{\mathbf{r}}\left(\frac{1}{c}\dot{L}_rU(1,2)+(L_r-L_M)U(2,2)+\frac{L_r}{c}WU(2,3)\right)\right\}\right]_{\text{ret}}\mathrm{d}S\\ &+\frac{1}{c}\int_{f=0}\left[\frac{1}{1-M_r}\frac{\partial}{\partial\tau}\{(\mathbf{L}-L_r\hat{\mathbf{r}})U(2,1)\}\right]_{\text{ret}}\mathrm{d}S\\ &-\frac{1}{c}\int_{f=0}\left[\frac{1}{1-M_r}\frac{\partial}{\partial\tau}\{L_r(\hat{\mathbf{r}}-\mathbf{M})U(2,2)\}\right]_{\text{ret}}\mathrm{d}S\\ &+\int_{f=0}[(\mathbf{L}-3L_r\hat{\mathbf{r}})U(3,1)]_{\text{ret}}\,\mathrm{d}S,\end{aligned} \tag{39}$$

where $\rho_0 U_n$ is defined as Q.

Eqs. (38) and (39) can be written in a short hand notation for convenience

$$4\pi\nabla p'_T(\mathbf{x},t) = I_1 + I_2, \tag{40}$$

$$4\pi\nabla p'_L(\mathbf{x},t) = I_3 + I_4 + I_5 + I_6, \tag{41}$$

where I_1–I_6 correspond to each of the integrals in Eqs. (38) and (39). Detailed forms of I_1–I_6 after performing the differentiation of variables with respect to the source time are given in Appendix A.

Eqs. (40) and (41), together with the definitions of I_1—I_6, will be referred to as formulation G1A and are the main result of this paper. The designation G1A is intended to parallel that of Farassat's formulation 1A, in which the observer time derivative is taken analytically inside the monopole and dipole integrals. Formulation G1A does not require numerical time differentiation of the integrals, and, as a retarded-time formulation, is well suited for subsonic source motion. Aside from the problem geometry, only the time-dependent input values or at most, numerical differentiation of them are required. Furthermore, it will be demonstrated with numerical examples that formulation G1A requires significantly less operations and computer memory than formulation G1. This will be discussed in detail later. The reduction of computational cost is important when the formulation is used for the scattering problem.

It is worthwhile to point out possible numerical error sources in the developed analytical formulations. Numerical errors can be associated with insufficient temporal and spatial resolution of the source and a numerical evaluation of integrals. An error analysis will be carried out in the following section. Other than these error sources, no other numerical errors associated with wave propagation, such as dissipation or dispersion errors that are important issues in computational fluid dynamics (CFD), are involved in the formulations because the solution obtained using the free-space Green's function is exact at the far field under the assumption of linear superposition.

4. Validation of the analytic formulations of the pressure gradient

The developed analytic formulations will be validated by comparison with exact solutions of the pressure gradient for both stationary and moving monopole sources. In the case of a moving source, both a stationary source in a moving stream and a moving source in a stationary stream will be considered.

4.1. Validation case 1: a stationary source

The first validation case is a stationary point monopole source problem. The three-dimensional inhomogeneous wave equation is given by

$$\Box^2 p'(\mathbf{x},t) = q(\mathbf{x},t). \tag{42}$$

A source which is concentrated at a point is given as

$$q(\mathbf{x},t) = Q(t)\delta(\mathbf{x}). \tag{43}$$

For a point monopole source with a single frequency ω, the source is given by

$$q(\mathbf{x},t) = A\mathrm{e}^{\mathrm{i}\omega t}\delta(\mathbf{x}), \tag{44}$$

where A is a complex constant.

The three-dimensional Green's function gives the solution of the acoustic pressure for a point monopole source located at the origin:

$$p'(r,t) = \frac{Q(t-r/c)}{4\pi r} = \frac{A\mathrm{e}^{\mathrm{i}\omega(t-r/c)}}{4\pi r}, \tag{45}$$

where $r = |\mathbf{x}-\mathbf{y}|$ and $t-r/c$ is called the retarded time.

Once the pressure is determined, the particle velocity can be calculated from it using the linearized momentum equation. The radial component of the equation gives

$$\rho_0 \frac{\partial u_r}{\partial t} = -\frac{\partial p'}{\partial r}. \tag{46}$$

The pressure gradient in the r direction is given by

$$\frac{\partial p'}{\partial r} = -\frac{A}{4\pi}\left\{\frac{\mathrm{i}\omega}{cr} + \frac{1}{r^2}\right\}\mathrm{e}^{\mathrm{i}\omega(t-r/c)}. \tag{47}$$

Substituting Eq. (47) into Eq. (46) gives

$$u_r(r,t) = \frac{A}{4\pi(\mathrm{i}w\rho_0)}\left\{\frac{\mathrm{i}\omega}{cr} + \frac{1}{r^2}\right\}\mathrm{e}^{\mathrm{i}\omega(t-r/c)}. \tag{48}$$

Eqs. (45) and (47) give the exact solutions of acoustic pressure and pressure gradient at an observer point. In order to validate the pressure gradient formulations implemented in PSU-WOPWOP, a permeable data surface enclosing the point source is used. Eqs. (45) and (48) yield the variables U_i and L_i on the surface. In the prediction, $A = 4\pi$ is used.

The spherical permeable surface used has a radius of 0.5 m and the polar azimuthal angle θ and polar angle ϕ are discretized into 36 and 18 panels, respectively.

Fig. 1 shows a comparison of the acoustic pressure at $r = 10$ m for the exact solution and prediction. Source frequency is $\omega = 10$ rad/s. The predicted result agrees very well with the exact solution. The order of the error for the peak value is less than 1%. This result demonstrates that the permeable surface prediction is correct.

Fig. 2 shows a comparison of the acoustic pressure gradient for the exact solution, the predictions with formulations G1 and G1A and the finite difference method. It can be seen the predictions match extremely well with the exact solution so that each line can barely be differentiated on this graph. This result confirms that the analytical formulations of the pressure gradient can be used to accurately compute the pressure gradient for a stationary source case.

Although we demonstrated that the analytical formulations are very successful, numerical error associated with the grid resolution of the source needs to be addressed. Fig. 3 shows the pressure gradient prediction for the stationary case depending on the mesh points on the permeable surface. Three test cases were used for the grid convergence test: 36×18 mesh points, 18×9 mesh points, 9×4 mesh points. It was found that the numerical error caused by the coarse grid resolution reduced the amplitude of the peaks.

4.2. Validation case 2: wind-tunnel case

The second validation problem is a "wind-tunnel case", where the source is stationary, but the flow is moving with a constant velocity of U. This test case is for the validation of the pressure gradient formulations in a moving source case.

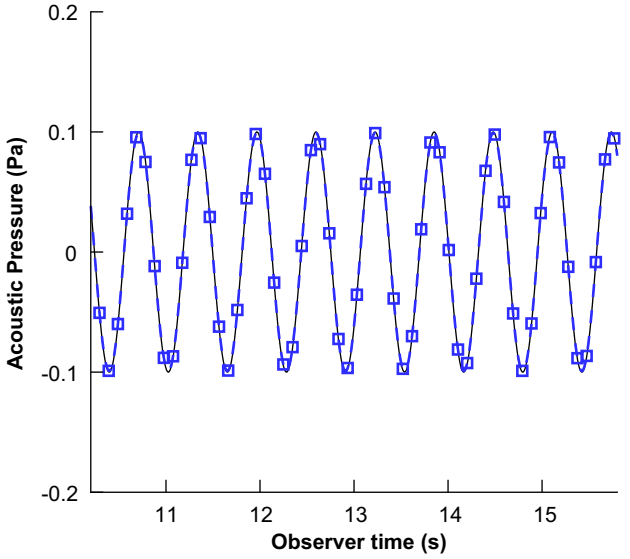

Fig. 1. Acoustic pressure comparison for a harmonic stationary source $\omega = 10\,\mathrm{rad/s}$; exact solution:——; prediction with the spherical permeable surface: — — □ — —.

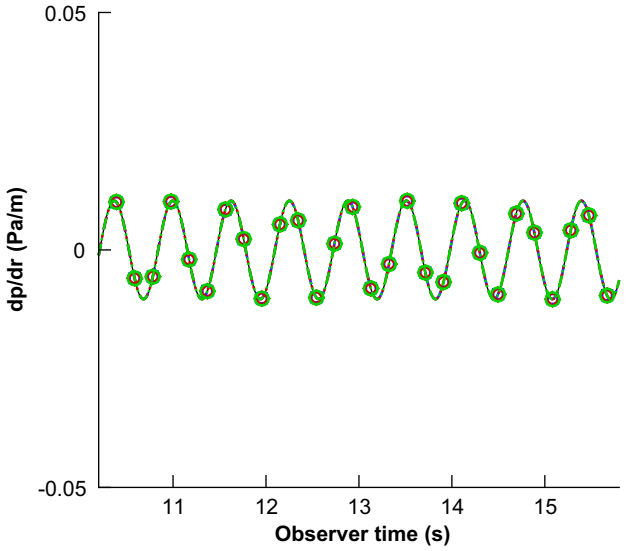

Fig. 2. Acoustic pressure gradient comparison for a harmonic stationary source $\omega = 10\,\mathrm{rad/s}$; exact solution: ——; formulation G1A: — — □ — —; formulation G1: — ▪ — ◇ — ▪ —; finite difference method: — ▪ — ○ — ▪ —.

The acoustic velocity potential for a stationary source in a uniform stream is written as

$$\left[\frac{1}{c^2}\frac{\mathrm{D}^2}{\mathrm{D}t^2} - \nabla^2\right]\phi'(\mathbf{x}, t) = 0, \tag{49}$$

where $\mathrm{D}/\mathrm{D}t$ is the material (or total) derivative operator and $\phi'(\mathbf{x}, t)$ is the velocity potential. The source and observer are stationary in a uniformly moving stream with a Mach number $M = U_0/c$.

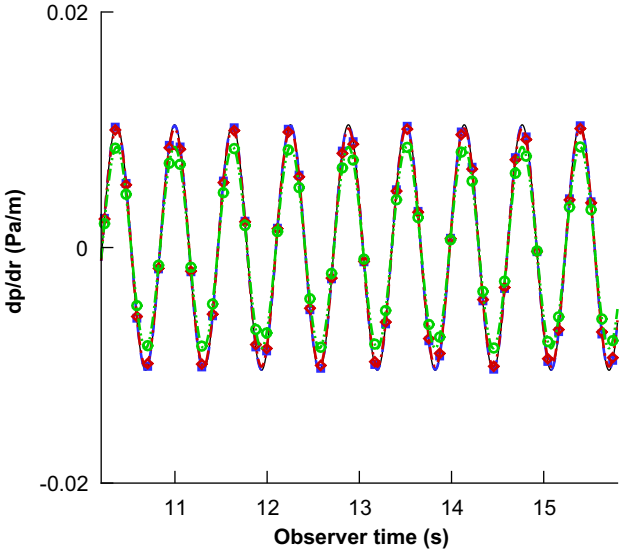

Fig. 3. Acoustic pressure gradient for a different mesh points used; exact solution: ——; prediction with 36×18 points: — — □ — —; prediction with 18×9 points: — - — ◇ — - —; prediction with 9×4 points: — - - — ○ — - - —.

The Green's function for the convective wave equation for a harmonic source gives the solution for the velocity potential. It is given by

$$\phi'(\mathbf{x},t) = \frac{A\beta^2}{4\pi\bar{R}}\exp\{\mathrm{i}k[\bar{R} - M\beta^2(x-x_s)]\}\exp\{-\omega t\}, \tag{50}$$

where

$$\bar{R} = \beta\sqrt{\beta^2(x-x_s)^2 + (y-y_s)^2 + (z-z_s)^2}, \tag{51}$$

and, $\beta = 1/\sqrt{1-M^2}$. The retarded time is given by

$$\tau^* = t - \frac{R}{c(1-M)^2}\left(M\cos\Theta + \sqrt{1-M^2\sin^2\Theta}\right), \tag{52}$$

where $R = \sqrt{(x-x_s)^2 + (y-y_s)^2 + (z-z_s)^2}$ and $\cos\Theta = (x-x_s)/R$.

The acoustic particle velocity can be obtained by the gradient of the velocity potential

$$\mathbf{v}'(\mathbf{x},t) = \nabla\phi'(\mathbf{x},t). \tag{53}$$

The acoustic pressure is described by the unsteady Bernoulli equation

$$p'(\mathbf{x},t) = \rho_0\left(\mathrm{i}\omega - U_0\frac{\partial}{\partial x}\right)\phi'(\mathbf{x},t). \tag{54}$$

The exact solution for the acoustic pressure gradient with respect to the x, y and z coordinates is given by

$$\frac{\partial p'}{\partial x} = \rho_0\left(\mathrm{i}\omega\frac{\partial\phi'}{\partial x} - U_0\frac{\partial^2\phi'}{\partial x^2}\right), \tag{55}$$

$$\frac{\partial p'}{\partial y} = \rho_0\left(\mathrm{i}\omega\frac{\partial\phi'}{\partial y} - U_0\frac{\partial^2\phi'}{\partial x\,\partial y}\right), \tag{56}$$

$$\frac{\partial p'}{\partial z} = \rho_0 \left(\mathrm{i}\omega \frac{\partial \phi'}{\partial z} - U_0 \frac{\partial^2 \phi'}{\partial x \, \partial z} \right). \tag{57}$$

Terms that are necessary for calculating the pressure gradient are provided in Appendix B.

The procedure of making the pressure gradient predictions is similar to that used for the stationary point monopole source. A spherical permeable surface enclosing a point source is created and flow passes by the surface with Mach number **M**. The pressure and velocity evaluated on the surface are passed to PSU-WOPWOP and used for the prediction of the pressure gradient. Again, $A = 4\pi$ is used in this problem.

Fig. 4 shows a comparison of the acoustic pressure at a point observer of $(100.0, 0.0, -5.0)$ for the prediction and the exact solution for Mach number $M = 0.5$ and 0.9 cases. The source frequency is $\omega = 10\,\mathrm{rad/s}$. The agreement between the FW–H prediction and the exact solution is excellent for both low and high Mach number cases. The order of the error for the peak is less than 1% for both cases.

Fig. 5 shows a comparison of the acoustic pressure gradient for the exact solution, the predictions with formulations G1 and G1A and the finite difference method. It can be seen the predictions match extremely well, such that the exact solution so that each line can barely be distinguished on this graph. In addition to validate the methodology, the result implies that the finite difference method, which is a purely numerical

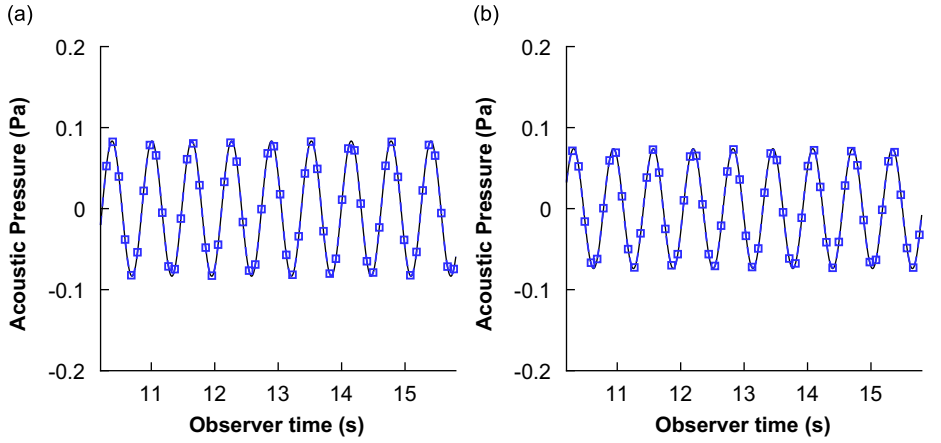

Fig. 4. Acoustic pressure comparison for a harmonic source $\omega = 10\,\mathrm{rad/s}$ embedded in a uniform stream: (a) $M = 0.5$, (b) $M = 0.9$; exact solution: ——; prediction with the spherical permeable surface: — — □ — —.

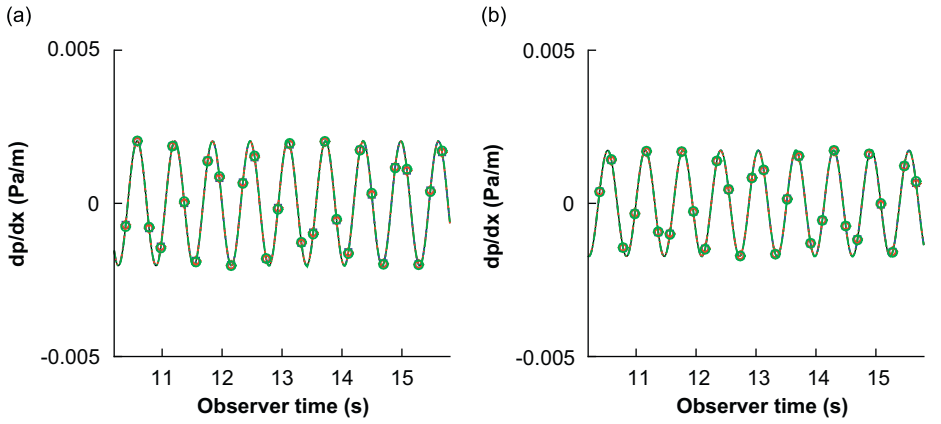

Fig. 5. Acoustic pressure gradient comparison for a harmonic source $\omega = 10\,\mathrm{rad/s}$ embedded in a uniform stream: (a) $M = 0.5$, (b) $M = 0.9$; exact solution: ——; formulation G1A: — — □ — —; formulation G1: — - — ◇ — - —; finite difference method: — - - — ○ — - - —.

method, can be used as a baseline for the validation of the pressure gradient formulations when the source motion is not linear and the exact solution for the pressure gradient is not available.

4.3. Validation case 3: a uniformly moving source

Now let us consider a monopole source with a strength of q moving uniformly in the x-direction with a velocity U in a stationary fluid. The wave equation for the acoustic pressure field generated by this moving point source is of the form

$$\Box^2 p'(\mathbf{x},t) = \frac{\partial}{\partial t} q(t)\delta(x-Ut)\delta(y)\delta(z), \tag{58}$$

where $q(t) = A\mathrm{e}^{\mathrm{i}\omega t}$. The linearized unsteady Bernoulli equation is given by

$$p'(\mathbf{x},t) = -\rho_0 \frac{\partial \phi'}{\partial t}, \tag{59}$$

where ϕ' is the velocity potential. Defining $\psi' = -\rho_0\phi'$, one obtains

$$\Box^2 \psi'(\mathbf{x},t) = q(t)\delta(x-Ut)\delta(y)\delta(z). \tag{60}$$

This equation can be solved in many different ways. Many researchers used a linear transformation of coordinates analogous to a Lorentz transformation. This is given in Ref. [17] in detail. This transformation enables the reduction of the problem to that of radiation from a stationary source, but it involves complicated mathematical manipulations. In the present work, the solution of Eq. (60) is more easily derived by using Farassat's formulation 1A for the integral solution of the FW–H equation.

Using the free-space Green's function and the properties of the δ function, the solution of Eq. (60) becomes

$$\psi'(\mathbf{x},t) = \left.\frac{q(\tau)}{4\pi r(1-M_r)}\right|_{\mathrm{ret}}, \tag{61}$$

where $q(\tau) = A\exp(\mathrm{i}\omega\tau)$.

The pressure can be written as

$$p' = \frac{\partial \psi'}{\partial t} = \frac{1}{1-M_r}\frac{\partial}{\partial \tau}\left[\frac{q(\tau)}{4\pi r(1-M_r)}\right]_{\mathrm{ret}} = \left[\frac{\dot{q}(\tau)}{4\pi r(1-M_r)^2}\right]_{\mathrm{ret}} + \left[\frac{q(\tau)(cM_r - cM^2)}{4\pi r^2(1-M_r)^3}\right]_{\mathrm{ret}}. \tag{62}$$

Eq. (62) is equivalent to the monopole noise term of Farassat's formulation 1A for a moving source with a constant velocity. The particle velocity is given by the gradient of the velocity potential

$$\mathbf{v}'(\mathbf{x},t) = \nabla\phi'(\mathbf{x},t) = -\frac{\nabla\psi'(\mathbf{x},t)}{\rho_0}, \tag{63}$$

where

$$\nabla\psi' = \left[\frac{A\mathrm{i}\omega q(\tau)\nabla\tau}{4\pi r(1-M_r)}\right]_{\mathrm{ret}} + q(\tau)\nabla\left\{\left[\frac{A}{4\pi r(1-M_r)}\right]_{\mathrm{ret}}\right\}. \tag{64}$$

The second part of Eq. (64) needs to be evaluated very carefully. It should be noted that

$$\nabla\left\{\left[\frac{A}{4\pi r(1-M_r)}\right]_{\mathrm{ret}}\right\} \neq \left[\nabla\left\{\frac{A}{4\pi r(1-M_r)}\right\}\right]_{\mathrm{ret}}. \tag{65}$$

Here the left-hand side means that the gradient operator is applied *after* the evaluation of the function at the retarded time. In contrast, the right-hand side of Eq. (65) is carried out *before* the retarded time is determined. This gives a wrong answer. To avoid making this mistake, it is useful to preform the gradient operation before the retarded-time relation is applied (i.e., before the $\delta(g)$ term in the free-space Green's function is integrated). For this case of a uniformly moving source, it is useful to express the denominator of Eq. (65) in terms of the observer position, initial source position, and the velocity

of the source. In this form, one obtains

$$r(1-M_r) = c(t-\tau) - M(x_1 - U\tau) = \sqrt{(x-x_s)^2 + (1-M^2)\{(y-y_s)^2 + (z-z_s)^2\}}, \tag{66}$$

where x, y and z are the observer coordinates and x_s, y_s and z_s are the initial source coordinates. Now the problem is given in only $\mathbf{x}$ and t variables and the explicit dependence on source space–time is eliminated. Now the second part of Eq. (64) becomes

$$q(\tau)\nabla\left\{\frac{1}{4\pi\sqrt{(x-x_s)^2 + (1-M^2)\{(y-y_s)^2 + (z-z_s)^2\}}}\right\}\Bigg|_t. \tag{67}$$

Once the exact solutions for the pressure and particle velocity are determined, these data on the permeable surface are used to evaluate formulations G1 and G1A in PSU-WOPWOP. The same permeable surface used with the previous validation cases is used here and $A = -4\rho_0\pi$ is used to match the strength of the monopole source with that for the wind-tunnel case.

Fig. 6 shows a comparison of the acoustic pressure at an observer located $(100.0, 0.0, -5.0)$ for both the prediction and the exact solution for Mach number $M = 0.5$ and 0.9 cases. The agreement between the FW–H prediction and the exact solution is excellent for both low and high Mach number cases. Again, the order of the error for the peak is less than 1%.

Fig. 7 shows a comparison of the acoustic pressure gradient for the exact solution, the predictions with formulations G1 and G1A and the finite difference method. The derivation of the exact solution for the pressure gradient for a moving source case requires heavy algebraic manipulations so the exact solution obtained from the validation case 2 (the moving stream case) is used since both approaches give identical results. The predictions are again in excellent agreement with the exact solution.

These results demonstrate that the pressure and pressure gradient obtained from a stationary source in a moving stream are identical with those predicted by a moving source in stationary fluid. The validation for a moving source is complete.

Fig. 8 shows the instantaneous pressure contour for a source wavelength $\lambda = 2\,\mathrm{m}$ and $M = 0.5$. The source is moving in the $-x$ direction. The Doppler effect of changing wavelength can be seen in the figure. Figs. 9–11 show contours of the pressure gradient. The contours of pressure gradient tend to lean toward the direction of the source motion.

5. Application of the analytic formulations of the pressure gradient to rotor noise

In this section, two representative calculations are performed to demonstrate the capability of the new formulations and to provide some indication of the efficiency and robustness of the formulations. The first

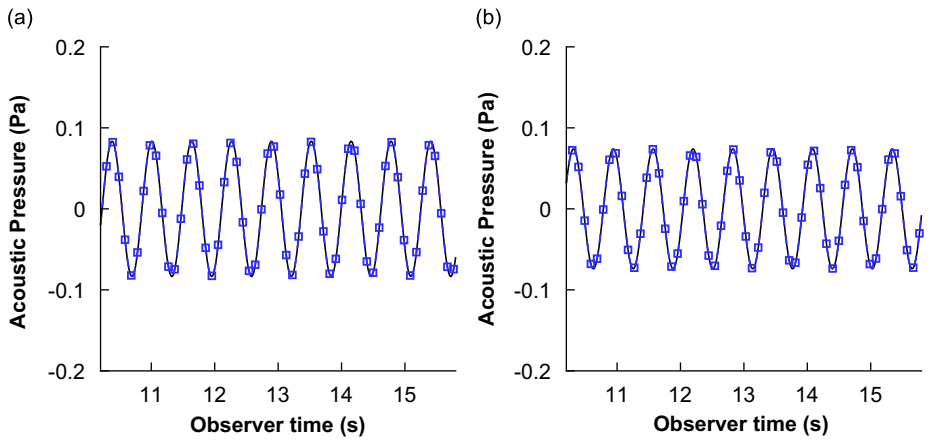

Fig. 6. Acoustic pressure comparison for a harmonic moving source $\omega = 10\,\mathrm{rad/s}$: (a) $M = 0.5$, (b) $M = 0.9$; exact solution: ——; prediction with the spherical permeable surface: — — □ — —.

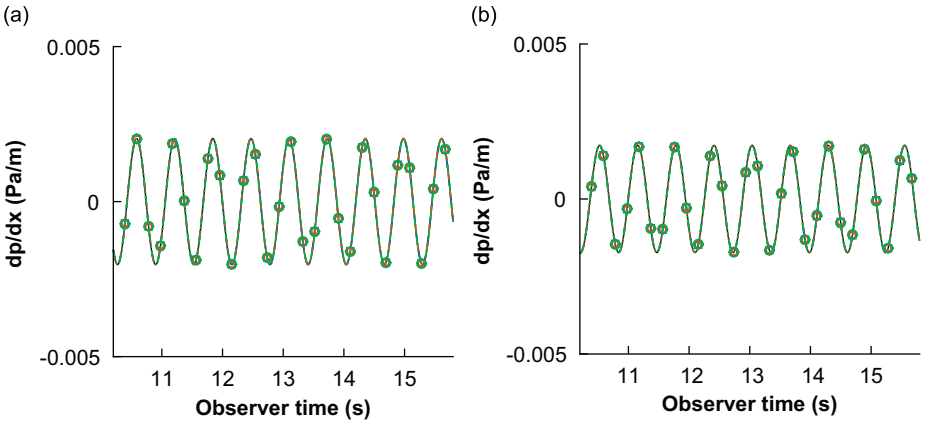

Fig. 7. Acoustic pressure gradient comparison for a moving harmonic source $\omega = 10\,\mathrm{rad/s}$: (a) $M = 0.5$, (b) $M = 0.9$; exact solution: ——; formulation G1A: — — □ — —; formulation G1: — - — ◇ — - —; finite difference method: — - - — ○ — - - —.

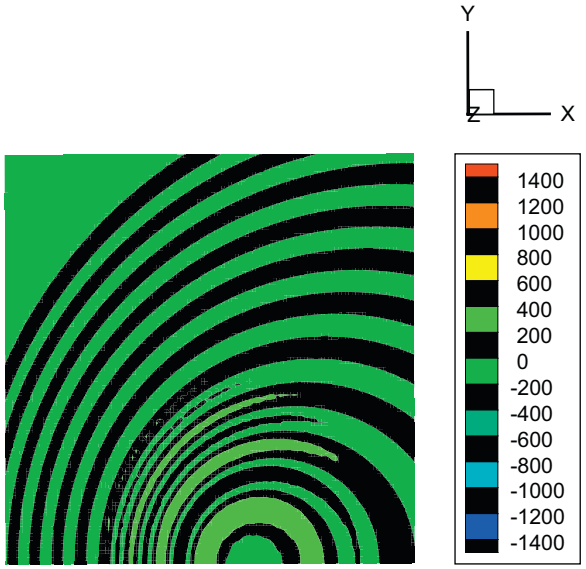

Fig. 8. Contour of the acoustic pressure at an instantaneous time for $M = 0.5$ and $\lambda = 2\,\mathrm{m}$. The source is positioned at $(0, 0, 0)$ and the boundary is $-10 \leqslant x \leqslant 10$, $0 \leqslant y \leqslant 20$, $z = -5$.

case considers a model-scale UH-1H rotor with untwisted blades operating in a non-lifting hover condition. This test enables simple and fast calculation for both the pressure and pressure gradient. The other test case is for the HART-I model rotor in a forward descent flight, which experiences blade–vortex interaction (BVI) high-frequency loading on the blades (although the CFD solution does not fully capture the BVI). Measured data are not available for the pressure gradient; therefore, the predicted pressure-gradient time histories using formulations G1 and G1A must be compared with a purely numerical calculation. The finite difference predictions are performed by computing the acoustic pressure at several points nearby the observer location and then using a second-order central finite difference in each of the three spatial directions.

5.1. Test case 1: UH-1H model rotor

A model scale rotor test, conducted by Boxwell et al. [18] in 1978 and later repeated by Purcell [19] in 1988, has been selected for the validation of the present analysis and code. The rotor was a one-seventh scale model

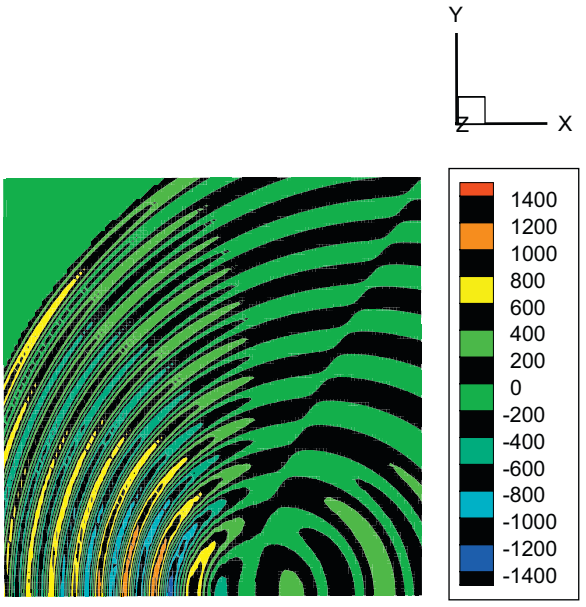

Fig. 9. Contour of $\partial p'/\partial x$ at an instantaneous time for $M = 0.5$ and $\lambda = 2$ m. The source is positioned at $(0, 0, 0)$ and the boundary is $-10 \leqslant x \leqslant 10$, $0 \leqslant y \leqslant 20$, $z = -5$.

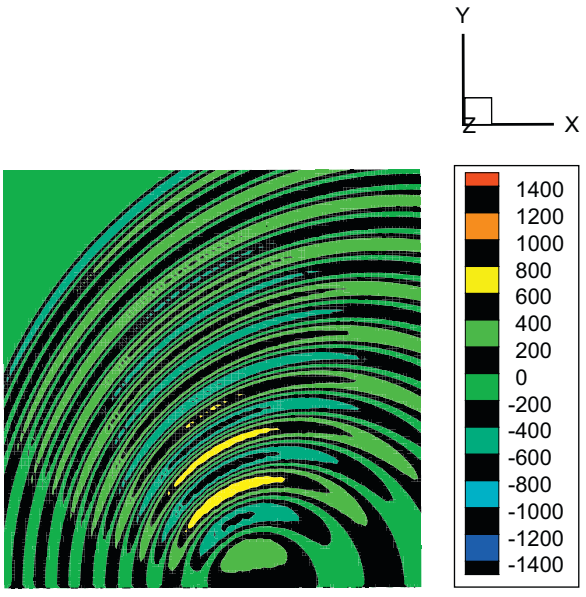

Fig. 10. Contour of $\partial p'/\partial y$ at an instantaneous time for $M = 0.5$ and $\lambda = 2$ m. The source is positioned at $(0, 0, 0)$ and the boundary is $-10 \leqslant x \leqslant 10$, $0 \leqslant y \leqslant 20$, $z = -5$.

of a UH-1H main rotor with straight, untwisted blades. The model rotor had an NACA 0012 airfoil section. The rotor radius R was 1.045 m with a chord of 7.62 cm. The model was run at several high-speed hover conditions with low thrust. The high-speed hover condition is not of particular interest for the validation of the pressure gradient; therefore, a tip Mach number of 0.6 is selected for the test case. For the hover noise calculation, an Euler solution reported by Baeder et al. [20,21] is used as input data. The Euler calculations were performed on a C-H grid; only the lower half of the grid was used in the CFD calculations by taking

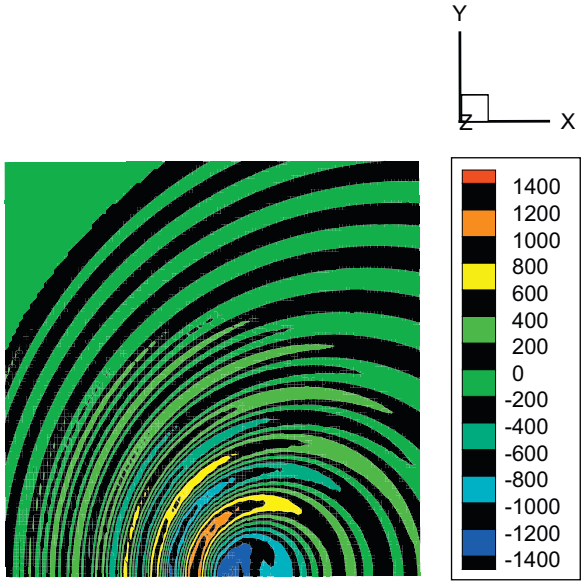

Fig. 11. Contour of $\partial p'/\partial z$ at an instantaneous time for $M = 0.5$ and $\lambda = 2$ m. The source is positioned at $(0, 0, 0)$ and the boundary is $-10 \leqslant x \leqslant 10$, $0 \leqslant y \leqslant 20$, $z = -5$.

advantage of the symmetry of the problem. The Euler calculations required approximately 80 min of CPU time on a Cray Y-MP. Details of the Euler calculations can be found in Refs. [20,22].

Comparisons of the pressure gradient are made for an in-plane microphone located $3.09R$ from the rotor hub for a stationary observer. Fig. 12 shows the total acoustic pressure and the pressure gradient with respect to the x, y, and z directions, respectively. The pressure gradient predicted by the two analytical formulations are compared to that obtained by the finite difference method. The agreement between the analytic formulations and the finite difference method is excellent for all components of the pressure gradient. A closer examination reveals that the analytical formulations provide much smoother results as compared to the finite difference method. The order of the error for the peak is 0.1%.

5.2. Test case 2: HART-I model rotor

The forward-flight capability of the new formulations and code is demonstrated for a four-bladed rotor representative of the HART-I model-scale test. This case focuses on unsteady blade loading and forward flight. The OVERFLOW CFD code was used to compute the unsteady flow field around the rotor [23,24]. A C-mesh topology was been used for the grid with a total grid system of 2.4 million points in the near-body region and 15.0 million points in the off-body region—in the coarse grid case. The turbulence model used the shear stress transport (SST) [25] $k-\omega$ by Menter. The rapid dissipation of blade–vortex strength makes the prediction of blade–vortex interactions with computational fluid dynamics (CFD) difficult. Although the CFD was not fully able to capture the BVI loading on the blades—and hence the peaks of predicted noise were considerably underpredicted as shown in Refs. [23,24]—the comparison of the new analytical formulations for pressure gradient with the finite difference method is still useful to demonstrate its implementation in PSU-WOPWOP.

As in the UH-1H examples, the finite difference result is compared to that of analytic formulations to validate the newly developed formulations. For this comparison, the observer is located below the rotor plane at a downstream position on the retreating side of the rotor. The observer is in motion with the rotor to simulate a wind-tunnel test. Although the absolute magnitude of the pressure gradient is unknown, confidence in both the derivation and implementation of the new formulations would be gained if all of the different methods agree.

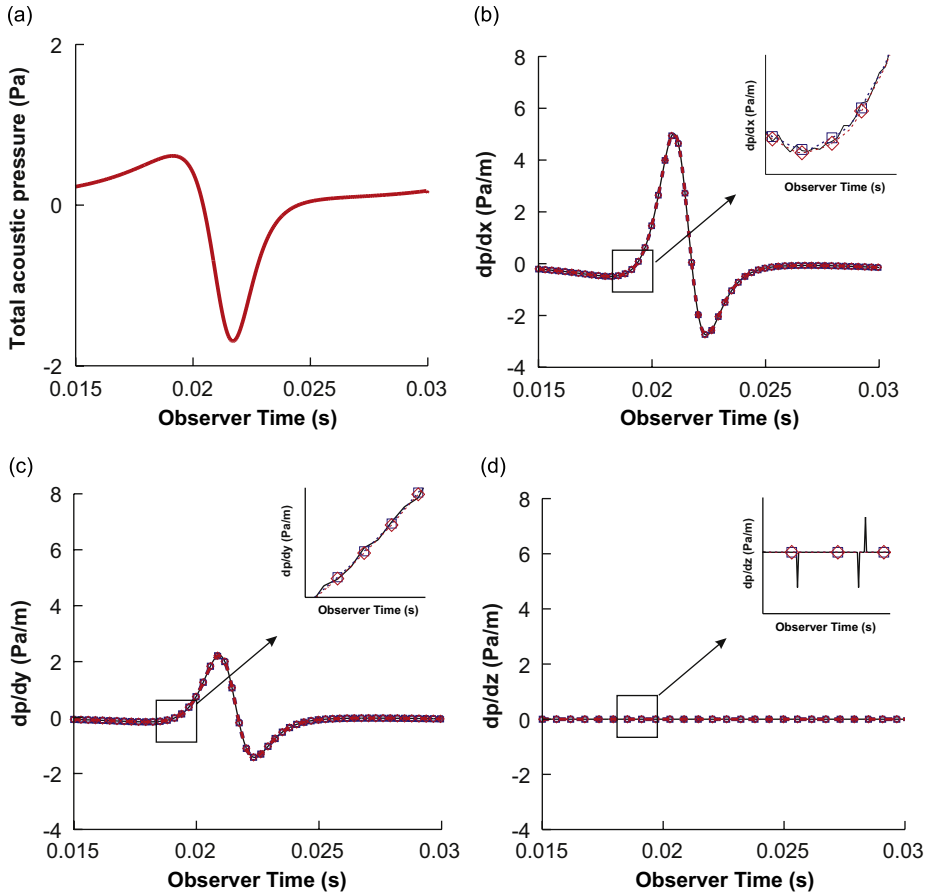

Fig. 12. Acoustic pressure and the components of the acoustic pressure gradient for the UH-1H model rotor operating in hover with $M_{tip} = 0.6$: (a) total acoustic pressure, (b) $\partial p'/\partial x$, (c) $\partial p'/\partial y$, (d) $\partial p'/\partial z$; finite difference method: ——; formulation G1A: — — □ — —; formulation G1: — ▪ — ◇ — ▪ —.

Fig. 13 shows the total acoustic pressure and a comparison of the pressure gradient at a moving observer for the HART-I rotor. The analytical formulations are in a good agreement with the finite difference method. Upon closer inspection (not shown), the finite difference result contains a high-frequency "jitter" that is thought to be of numerical origin. The analytical formulations do not exhibit the same "jitter." In some other cases with a moving observer (not shown) it was found that the acoustic pressure gradient predicted by formulation G1 was sensitive to the method of computing the observer time and position. This has not been studied extensively as formulation G1A does not suffer in this regard, and also requires less computational effort.

Table 1 shows a comparison of computational times for formulation 1A (as a reference), formulations G1A and G1, and the finite difference method. The finite difference method requires 7 times as much time as formulation 1A but formulation G1A only required 3 times as much computation time as formulation 1A. Formulation G1 requires approximately 5 times as much computation time as formulation 1A or 60 percent more computation time than formulation G1A. This demonstrates the significant computational savings of both of the analytical formulations and the superiority of formulation G1A.

6. Concluding remarks

In this paper, two analytical formulations for the determination of the acoustic pressure gradient have been developed and validated by comparison with available exact solutions for both stationary and moving point

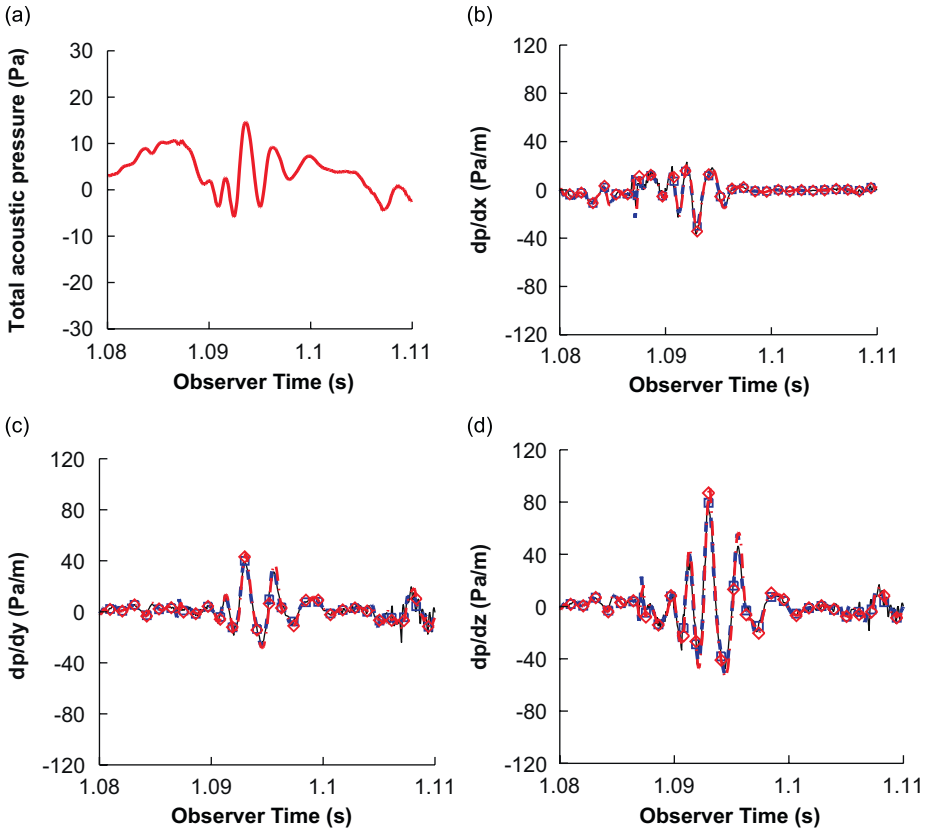

Fig. 13. Acoustic pressure and the components of the acoustic pressure gradient for the HART-I rotor operating in a BVI flight condition. (a) total acoustic pressure, (b) $\partial p'/\partial x$, (c) $\partial p'/\partial y$, (d) $\partial p'/\partial z$; finite difference method: ——; formulation G1A: — — □ — —; formulation G1: — - — ◇ — - —.

Table 1
Comparison of computational time for the HART rotor with permeable surface

Formulation 1A	Formulation G1A	Formulation G1	Finite difference method
11.5 (s)	31.7 (s)	49.4 (s)	79.0 (s)

monopole sources. It has been demonstrated that the analytical formulations agree very well with the exact solution for three different cases. The fact that all three approaches give essentially the same results—although they are quite different in expression and implementation—gives confidence that both the derivation and implementation have been performed correctly. The formulations are applied to rotor blades for both hovering and forward-flight conditions. The analytical formulations eliminate numerical oscillations, which are present in the finite difference method and result in very smooth predictions.

It has been found that formulation G1, which evaluates the observer time differentiation of the integrals, is a relatively simple formulation but is somewhat more difficult to implement in PSU-WOPWOP due to the observer time differentiation of the acoustic integrals. Furthermore, in at least one case, it was found to be sensitive to the choice of numerical algorithm used to find the observer time and location. In contrast, formulation G1A, which takes the time derivatives inside the integrals, is a somewhat more complicated formulation. Nevertheless, it yields improved computational efficiency and perhaps robustness by avoiding the numerical time differentiation of the acoustic integrals. Numerical tests show that formulation G1A is the fastest and the most efficient algorithm for computing the acoustic pressure gradient. This is important for use

in calculation of the acoustic scattering, which may require several thousand pressure gradient calculations at the collocation points on the scattering body.

Acknowledgments

This research was supported by Vertical Lift Research Center of Excellence (VLRCOE) under agreement No. W911W6-2-0008, task PS 1.9 and by NASA Langley Research Center under NASA purchase order NNL05AD50P.

Appendix A. Formulation G1A for the analytical pressure gradient

Five final equations of formulation G1A for the analytical pressure gradient are given as follows:

$$I_1 = -\frac{1}{c}\int_{f=0}[\hat{\mathbf{r}}\{\ddot{Q}U(1,3)+(3\dot{Q}W+Q\dot{W})U(2,4)+3QW^2U(3,5)\} - c\mathbf{M}\{\dot{Q}U(2,3)+QWU(3,4)\}]_{\text{ret}}\,\mathrm{d}S, \tag{A.1}$$

$$I_2 = \int_{f=0}[(\mathbf{M}-\hat{\mathbf{r}})\dot{Q}U(2,3)+(-cM_r\hat{\mathbf{r}}+c\mathbf{M}+r\dot{\mathbf{M}})QU(3,3) + 2(\mathbf{M}-\hat{\mathbf{r}})QWU(3,4)]_{\text{ret}}\,\mathrm{d}S, \tag{A.2}$$

$$\begin{aligned} I_3 = -\frac{1}{c^2}\int_{f=0}&[\hat{\mathbf{r}}(\ddot{L}_r+\dot{L}_{\dot{r}})U(1,3) \\ &+ c\{-\mathbf{M}\dot{L}_r-(-\dot{L}_r+\dot{L}_M+L_{\dot{M}})\hat{\mathbf{r}}\}U(2,3)]+\hat{\mathbf{r}}\{3\dot{L}_rW+L_r\dot{W}\}U(2,4) \\ &+ c^2\{(2L_rM_r-L_M(1+Mr))\hat{\mathbf{r}}-(L_r-L_M)\mathbf{M}\}U(3,3) \\ &+ c\{(L_r(M_r+2)-3L_M)W\hat{\mathbf{r}}-L_rW\mathbf{M}\}U(3,4)+3L_rW^2\hat{\mathbf{r}}U(3,5)]_{\text{ret}}\,\mathrm{d}S, \end{aligned} \tag{A.3}$$

$$I_4 = \frac{1}{c}\int_{f=0}[(\dot{\mathbf{L}}-\dot{L}_r\hat{\mathbf{r}})U(2,2)-c\{(3L_rM_r-L_M)\hat{\mathbf{r}}-L_r\mathbf{M}-M_r\mathbf{L}\}U(3,2) + (\mathbf{L}-L_r\hat{\mathbf{r}})WU(3,3)]_{\text{ret}}\,\mathrm{d}S, \tag{A.4}$$

$$I_5 = -\frac{1}{c}\int_{f=0}[\{\dot{L}_r(\hat{\mathbf{r}}-\mathbf{M})-L_r\dot{\mathbf{M}}\}U(2,3) + c\{\hat{\mathbf{r}}(2L_rM_r-L_M)-\mathbf{M}(M_rL_r-L_M+L_r)\}U(3,3) + 2L_r(\hat{\mathbf{r}}-\mathbf{M})WU(3,4)]_{\text{ret}}\,\mathrm{d}S, \tag{A.5}$$

$$I_6 = \int_{f=0}[(\mathbf{L}-3L_r\hat{\mathbf{r}})U(3,1)]_{\text{ret}}\,\mathrm{d}S. \tag{A.6}$$

Recall that for an impermeable surface,

$$Q = \rho_0 v_n, \tag{A.7}$$

$$L = P_{ij}\hat{n}_j, \tag{A.8}$$

and for a permeable surface,

$$Q = \rho_0 v_n + \rho(u_n - v_n), \tag{A.9}$$

$$L = P_{ij}\hat{n}_j + \rho u_i(u_n - v_n). \tag{A.10}$$

Also note that a dot on the main variables does not imply differentiation of any of the associated vectors implied by the subscripts. Subscripts other than i and j are a short hand for the inner product of the main

quantity with the vector represented by the subscript. The derivative of acceleration, which is called a jerk, and second derivative of normal unit vector are evaluated numerically in this work.

Appendix B. Exact solution for the pressure gradient for a moving stream case

Terms that are necessary to evaluate the exact solution for the pressure gradient for a moving stream case are given as follows:

$$\frac{\partial \phi'}{\partial x} = \phi' \left\{ -\frac{1}{\bar{R}} \frac{\partial \bar{R}}{\partial x} + \mathrm{i}k \left(\frac{\partial \bar{R}}{\partial x} - M\gamma^2 \right) \right\}, \tag{B.1}$$

$$\frac{\partial \phi'}{\partial y} = \phi' \left\{ -\frac{1}{\bar{R}} \frac{\partial \bar{R}}{\partial y} + \mathrm{i}k \frac{\partial \bar{R}}{\partial y} \right\}, \tag{B.2}$$

$$\frac{\partial \phi'}{\partial z} = \phi' \left\{ -\frac{1}{\bar{R}} \frac{\partial \bar{R}}{\partial z} + \mathrm{i}k \frac{\partial \bar{R}}{\partial z} \right\}, \tag{B.3}$$

$$\frac{\partial^2 \phi'}{\partial x^2} = \frac{\partial \phi'}{\partial x} \left\{ -\frac{1}{\bar{R}} \frac{\partial \bar{R}}{\partial x} + \mathrm{i}k \left(\frac{\partial \bar{R}}{\partial x} - M\gamma^2 \right) \right\} + \phi' \left\{ \frac{1}{\bar{R}^2} \left(\frac{\partial \bar{R}}{\partial x} \right)^2 - \frac{1}{\bar{R}} \frac{\partial^2 \bar{R}}{\partial x^2} + \mathrm{i}k \frac{\partial^2 \bar{R}}{\partial x^2} \right\}, \tag{B.4}$$

$$\frac{\partial^2 \phi'}{\partial x \partial y} = \frac{\partial \phi'}{\partial y} \left\{ -\frac{1}{\bar{R}} \frac{\partial \bar{R}}{\partial x} + \mathrm{i}k \left(\frac{\partial \bar{R}}{\partial x} - M\gamma^2 \right) \right\} + \phi' \left\{ \frac{1}{\bar{R}^2} \frac{\partial \bar{R}}{\partial x} \frac{\partial \bar{R}}{\partial y} - \frac{1}{\bar{R}} \frac{\partial^2 \bar{R}}{\partial x \partial y} + \mathrm{i}k \frac{\partial^2 \bar{R}}{\partial x \partial y} \right\}, \tag{B.5}$$

$$\frac{\partial^2 \phi'}{\partial x \partial z} = \frac{\partial \phi'}{\partial z} \left\{ -\frac{1}{\bar{R}} \frac{\partial \bar{R}}{\partial x} + \mathrm{i}k \left(\frac{\partial \bar{R}}{\partial x} - M\gamma^2 \right) \right\} + \phi' \left\{ \frac{1}{\bar{R}^2} \frac{\partial \bar{R}}{\partial x} \frac{\partial \bar{R}}{\partial z} - \frac{1}{\bar{R}} \frac{\partial^2 \bar{R}}{\partial x \partial z} + \mathrm{i}k \frac{\partial^2 \bar{R}}{\partial x \partial z} \right\}, \tag{B.6}$$

where

$$\frac{\partial \bar{R}}{\partial x} = \frac{\gamma^3 (x - x_s)}{\sqrt{\gamma^2 (x - x_s)^2 + (y - y_s)^2 + (z - z_s)^2}}, \tag{B.7}$$

$$\frac{\partial^2 \bar{R}}{\partial x^2} = \frac{\gamma^3}{\sqrt{\gamma^2 (x - x_s)^2 + (y - y_s)^2 + (z - z_s)^2}} - \frac{\gamma^5 (x - x_s)^2}{\left(\sqrt{\gamma^2 (x - x_s)^2 + (y - y_s)^2 + (z - z_s)^2} \right)^3}, \tag{B.8}$$

$$\frac{\partial^2 \bar{R}}{\partial x \partial y} = -\frac{\gamma^3 (x - x_s)(y - y_s)}{\left(\sqrt{\gamma^2 (x - x_s)^2 + (y - y_s)^2 + (z - z_s)^2} \right)^3}, \tag{B.9}$$

$$\frac{\partial^2 \bar{R}}{\partial x \partial z} = -\frac{\gamma^3 (x - x_s)(z - z_s)}{\left(\sqrt{\gamma^2 (x - x_s)^2 + (y - y_s)^2 + (z - z_s)^2} \right)^3}. \tag{B.10}$$

References

[1] N. Atalla, S. Glegg, A ray-acoustics approach to fuselage scattering of rotor noise, AIAA Paper 90-4013, *AIAA 13th Aeroacoustics Conference*, Tallahassee, FL, 1990.

[2] N. Atalla, S. Glegg, Ray-acoustics approach to fuselage scattering of rotor noise, *Journal of the American Helicopter Society* 38 (3) (1993) 56–63.

[3] O.A. Laik, P.J. Morris, Direct simulation of acoustic scattering by two- and three-dimensional bodies, *Journal of Aircraft* 37 (1) (2000) 68–75.
[4] M.H. Dunn, A.F. Tinetti, Aeroacoustic scattering via the equivalent source method, AIAA Paper 2004-2937, *AIAA 10th AIAA/CEAS Aeroacoustics Conference*, Manchester, UK, 2004.
[5] M.K. Myers, J.S. Hausmann, Computation of acoustic scattering from a moving rigid surface, *Journal of the Acoustical Society of America* 91 (5) (1992) 2594–2605.
[6] W. Jeon, D. Lee, A numerical study on the flow and sound fields of centrifugal impeller located near a wedge, *Journal of Sound and Vibration* 266 (4) (2003) 785–804.
[7] J.E. Ffowcs Williams, D.L. Hawkings, Sound generated by turbulence and surfaces in arbitrary motion, *Philosophical Transactions of the Royal Society A* 264 (1151) (1969) 321–342.
[8] G.A. Brès, Modeling the Noise of Arbitrary Maneuvering Rotorcraft: Analysis and Implementation of the psu-wopwop Noise Prediction Code, MS Thesis, Department of Aerospace Engineering, The Pennsylvania State University, June 2002.
[9] G. Perez, Investigation of the Influence of Maneuver on Rotorcraft Noise, MS Thesis, Department of Aerospace Engineering, The Pennsylvania State University, June 2002.
[10] K.S. Brentner, G. Perez, G.A. Brès, H.E. Jones, Maneuvering rotorcraft noise prediction, *Journal of Sound and Vibration* 39 (3–5) (2003) 719–738.
[11] K.S. Brentner, Prediction of helicopter discrete frequency rotor noise—a computer program incorporating realistic blade motions and advanced acoustic formulation, NASA TM 87721, 1986.
[12] F. Farassat, Derivation of formulations 1 and 1a of farassat, NASA TM 2007-214853, 2007.
[13] F. Farassat, K.S. Brentner, The derivation of the gradient of the acoustic pressure on a moving surface for application to the fast scattering code (fsc), Technical Report TM 2005-213777, NASA, July 2005.
[14] F. Farassat, Introduction to generalized functions with applications in aerodynamics and aeroacoustics (corrected copy (April 1996) available at http://techreports.larc.nasa.gov/ltrs/PDF/tp3428.pdf), NASA Technical Paper 3428, 1994.
[15] I.M. Gel'fand, G.E. Shilov, Generalized Functions: Properties and Operations, Vol. 1, Academic Press, Inc., 11 Fifth Avenue, New York 3, New York, 1964 (translated by Eugene Saletan, Department of Physics, Northeastern University, Boston, MA).
[16] R.P. Kanwal, *Generalized Functions—Theory and Applications*, third ed., Birkhauser, Boston, 2004.
[17] P.M. Morse, K.U. Ingard, *Theoretical Acoustics*, first ed., McGraw-Hill, Inc., New Jersey, 1968.
[18] D.A. Boxwell, Y.H. Yu, F.H. Schmitz, Hovering impulsive noise: some measured and calculated results, *Vertica* 3 (1) (1979) 35–45 also in NASA CP-2052-PT-1, 1978.
[19] T.W. Purcell, CFD and transonic helicopter sound, *Fourteenth European Rotorcraft Forum*, Milan, Italy, 1988, Paper 2.
[20] J.D. Baeder, J.M. Gallman, Y.H. Yu, A computational study of aeroacoustics of rotors in hover, *American Helicopter Society 49th Annual Forum*, St. Louis, MO, 1993.
[21] J.D. Baeder, J.M. Gallman, Y.H. Yu, A computational study of aeroacoustics of rotors in hover, *Journal of the American Helicopter Society* 42 (1) (1997) 39–53.
[22] J.D. Baeder, Euler solutions to nonlinear acoustics of non-lifting rotor blades, *American Helicopter Society and Royal Aeronautical Society International Technical Specialists Meeting: Rotorcraft Acoustics and Rotor Fluid Dynamics*, Valley Forge, PA, 1991.
[23] S.M. Makinen, M. Hill, F. Gandhi, L.N. Long, A study of higher harmonic airloads for helicopter rotors in descent flight with computational fluid dynamics, *62nd AHS Forum of the American Helicopter Society*, Phoenix, Arizona, 2006.
[24] S. Lee, K.S. Brentner, C.C. Hennes, B.T. Flynt, J.N. Theron, E.P.N. Duque, Investigation of the accuracy requirement for permeable surfaces used in rotor noise prediction, *62nd AHS Forum of the American Helicopter Society*, Phoenix, Arizona, 2006.
[25] F.R. Menter, C.L. Rumsey, Assessment of two-equation turbulence models for transonic flows, AIAA Paper 94-2343, 1994.